Editors' Suggestion

Double-dome superconductivity under pressure in the V-based kagome metals AV_3Sb_5 (A = Rb and K)

C. C. Zhu,[1,*] X. F. Yang,[1,*,†] W. Xia,[2,3,*] Q. W. Yin,[4,*] L. S. Wang,[1] C. C. Zhao,[1] D. Z. Dai,[1] C. P. Tu,[1] B. Q. Song,[1] Z. C. Tao,[2] Z. J. Tu,[4] C. S. Gong,[4] H. C. Lei,[4,‡] Y. F. Guo,[2,§] and S. Y. Li[1,5,6,‖]

[1]*State Key Laboratory of Surface Physics, Department of Physics, Fudan University, Shanghai 200438, China*
[2]*School of Physical Science and Technology, ShanghaiTech University, Shanghai 201210, China*
[3]*ShanghaiTech Laboratory for Topological Physics, Shanghai 201210, China*
[4]*Department of Physics and Beijing Key Laboratory of Opto-electronic Functional Materials and Micro-nano Devices, Renmin University of China, Beijing 100872, China*
[5]*Collaborative Innovation Center of Advanced Microstructures, Nanjing 210093, China*
[6]*Shanghai Research Center for Quantum Sciences, Shanghai 201315, China*

(Received 9 June 2021; revised 4 February 2022; accepted 4 March 2022; published 17 March 2022)

We present high-pressure resistance measurements on the newly discovered V-based superconductors AV_3Sb_5 (A = Rb and K), which have an ideal kagome lattice of vanadium. Two superconducting domes under pressure are observed in both compounds, as previously observed in their sister compound CsV_3Sb_5. For RbV_3Sb_5, the T_c increases from 0.93 K at ambient pressure to a maximum of 4.15 K at 0.38 GPa in the first dome. The second superconducting dome has the highest T_c of 1.57 K at 28.8 GPa. KV_3Sb_5 displays a similar double-dome phase diagram, however, its two maximum T_cs are lower, and the T_c drops faster in the second dome than RbV_3Sb_5. An integrated temperature-pressure phase diagram of AV_3Sb_5 (A = Cs, Rb, and K) is constructed, showing that the ionic radius of the intercalated alkali-metal atoms has a significant effect. Our work demonstrates that double-dome superconductivity under pressure is a common feature of these V-based kagome metals.

DOI: 10.1103/PhysRevB.105.094507

The materials with geometrically frustrated kagome lattice, depending on the degree of electron filling, host a wide range of intriguing physics, including quantum spin liquid, charge density wave (CDW), topological states, and superconductivity [1–7]. Recently, a new family of V-based kagome-lattice compounds AV_3Sb_5 (A = Cs, Rb, and K) was discovered [8]. The CDW order manifests in magnetic susceptibility, resistivity, and specific heat at 94, 103, and 78 K for A = Cs, Rb, and K, respectively [9–12]. At low temperature, these compounds also show superconductivity with superconducting transition temperature (T_c) of 2.5, 0.92, and 0.93 K for A = Cs, Rb, and K [9–11]. Interestingly, the scanning tunneling microscope (STM) study demonstrates a topological charge order in KV_3Sb_5 [12], which may cause the giant anomalous Hall effect [13] and possibly unconventional superconductivity [12]. The angle-resolved photoemission spectroscopy (ARPES) and density-functional theory demonstrated the existence of Z_2 nontrivial topological band structure in CsV_3Sb_5 [9].

For the superconducting gap structure in CsV_3Sb_5, while thermal conductivity measurements suggested nodal superconductivity [14], penetration depth and nuclear magnetic resonance (NMR) measurements claimed nodeless s-wave superconductivity [15,16]. The latest ultralow temperature STM measurements show both nodal and nodeless gaps [17] in this superconductor with multiple Fermi surfaces [18]. Theoretically, dominant f-wave triplet superconducting order, succeeded by d-wave singlet pairing for stronger coupling was found over a large range of coupling strength [19]. In this context, the exact locations of the gap nodes in CsV_3Sb_5 still need to be identified.

Meanwhile, two superconducting domes were observed in CsV_3Sb_5 under pressure, together with the nodal superconductivity, further indicating unconventional superconductivity in CsV_3Sb_5 [14]. The origin of the first dome in CsV_3Sb_5 is likely related to the CDW instability, due to the competition between CDW and superconductivity [14,20]. The second superconducting dome was attributed to a pressure-induced Lifshitz transition and enhanced electron-phonon coupling in CsV_3Sb_5 [21,22]. To understand this double-dome phase diagram, it will be interesting to study AV_3Sb_5 (A = Rb and K) under pressure and compare with CsV_3Sb_5.

In this paper, we performed high-pressure resistance measurements on AV_3Sb_5 (A = Rb and K) up to 50 GPa. A clear double-dome superconductivity was revealed in the temperature-pressure phase diagram of both compounds, as observed in CsV_3Sb_5. The ionic radius of the intercalated alkali-metal atoms apparently affects the phase diagram of AV_3Sb_5. We discuss the possible pairing mechanism under the two superconducting domes.

Single crystal of AV_3Sb_5 (A = Rb and K) were grown from K ingot (purity 99.8%) or Rb (purity 99.75%), V powder

*These authors contributed equally to this work.
†yangxiaofan@fudan.edu.cn
‡hlei@ruc.edu.cn
§guoyf@shanghaitech.edu.cn
‖shiyan_li@fudan.edu.cn

(purity 99.9%), Sb powder (purity 99.999%) through the self-flux method [8]. For RbV_3Sb_5, the eutectic mixture of RbSb and Rb_3Sb_7 was mixed with VSb_2 to form a composition with 50 at.% A_xSb_y (A = Rb and K) and 50 at.% VSb_2 approximately. The mixture was loaded into an alumina crucible, which was sealed in a quartz ampoule under partial argon atmosphere followed with heating to 1273 K by taking 12 h and kept there for 24 h. Subsequently, the temperature was cooled down to 1173 K at 50 K/h and further to 923 K with a slow rate. Finally, the ampoule was taken out from the furnace and decanted with a centrifuge to separate RbV_3Sb_5 single crystal from the flux. Analogous reactions were performed for KV_3Sb_5. The x-ray diffraction (XRD) was performed using powder x-ray diffractometer (D8 Advance, Bruker) with Cu $K\alpha$ radiation (wave length $\lambda = 1.5418$ Å).

High pressure was generated by a diamond anvil cell (DAC) made from Be-Cu alloy with two opposite diamond anvils. The diamonds with 300 μm culets were used for this experiment. Several pieces of small single crystals (less than 100 μm in size) were loaded on the NaCl powder, which were employed as the pressure transmitting medium. Subsequently, four electrodes of 4-μm-thick platinum thin foils were laid on the sample. With applying pressure, the small single crystals were crashed into powder and compressed together solidly, allowing a standard ohmic contact between sample and electrodes. The solid pressure transmitting medium provides a quasihydrostatic condition. The Be-Cu plate was used as gasket and cubic boron nitride served as insulating material. The pressure inside the DAC was scaled by monitoring the ruby fluorescence at room temperature each time before and after the measurement [23]. High-pressure resistance of AV_3Sb_5 (A = Rb and K) were measured in a physical property measurement system (PPMS, Quantum Design) and a ^{3}He cryostat with van der Pauw method.

As depicted in Figs. 1(a) and 1(b), AV_3Sb_5 (A = Rb and K) shows a layered structure with hexagonal symmetry ($P6/mmm$, No. 191). V ions are coordinated by Sb atoms, forming slabs with ideal kagome structure. The V-Sb layers are stacked along c axis separated by alkali-metal layers. The lattice constant c is 9.073(3) Å and 8.943(1) Å for RbV_3Sb_5 and KV_3Sb_5, respectively [8]. Figures 1(c) and 1(d) show XRD patterns of AV_3Sb_5 single crystals, in which only (00l) Bragg peaks can be observed, indicating that the largest natural surface of AV_3Sb_5 (A = Rb and K) single crystals is the ab plane. Typical resistivity curves of AV_3Sb_5 (A = Rb and K) single crystals at ambient pressure are plotted in Figs. 1(e) and 1(f). The residual resistivity ratio $RRR = \rho(300\ \mathrm{K})/\rho(1.5\ \mathrm{K})$ is 42 and 51 for RbV_3Sb_5 and KV_3Sb_5, respectively, suggesting high quality of the samples. A kink is observed at 100 K for RbV_3Sb_5 and 75 K for KV_3Sb_5, corresponding to the CDW transition as reported previously [10–12]. The T_c defined at 10% drop of normal-state resistance ($T_c^{10\%}$) is 0.93 and 1.24 K for RbV_3Sb_5 and KV_3Sb_5, respectively, as shown in the insets of Figs. 1(e) and 1(f), consistent with previous reports [10,11].

Figure 2(a) presents the low-temperature resistance of RbV_3Sb_5 in a pressure range of 0.38–9.35 GPa. The $T_c^{10\%}$ of RbV_3Sb_5 remarkably increases from 0.93 K at ambient pressure to 4.15 K at 0.38 GPa, then shifts to lower temperature with increasing pressure until reaches to 0.86 K at 9.35 GPa,

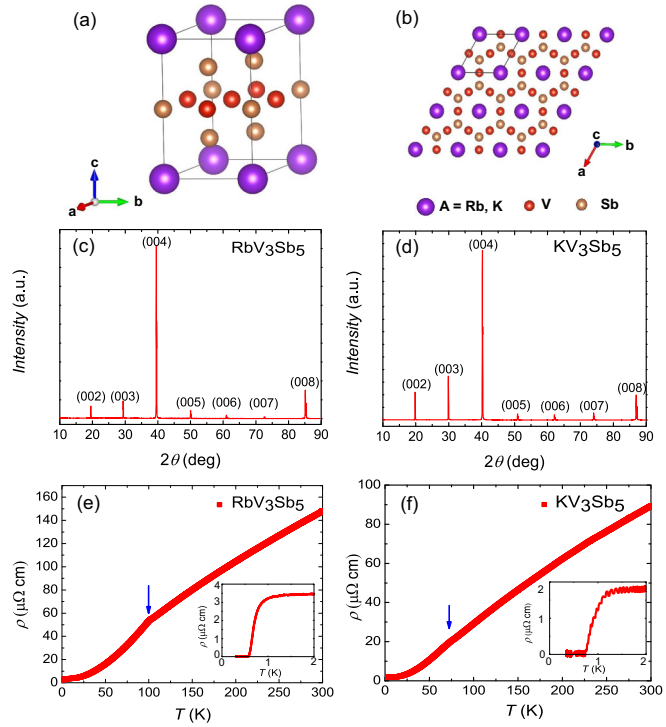

FIG. 1. (a) Crystal structure of AV_3Sb_5 (A = Rb and K). The A, V, Sb atoms are presented as purple, orange, and yellow balls, respectively. (b) Top view of the crystal structure, which shows the kagome lattice of vanadium. (c) and (d) X-ray diffraction pattern for the largest surface of the AV_3Sb_5 (A = Rb and K) single crystals. (e) and (f) Resistivity curves for RbV_3Sb_5 and KV_3Sb_5 single crystals, respectively, at ambient pressure. Blue arrows denote the CDW transitions. Insets of (e) and (f): superconducting transitions for AV_3Sb_5 (A = Rb and K).

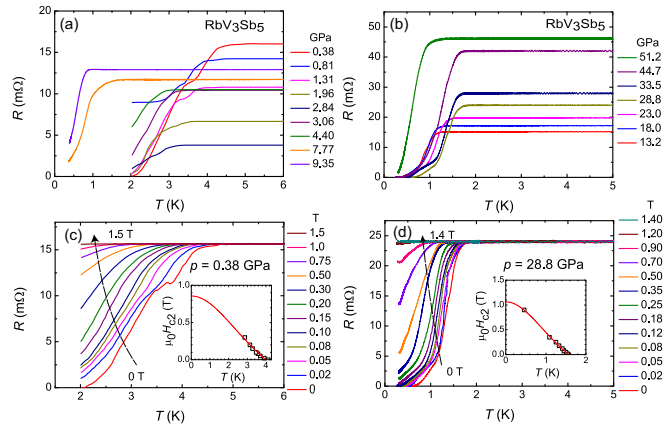

FIG. 2. (a) and (b) Temperature dependence of resistance for RbV_3Sb_5 under various pressures up to 51.2 GPa. (c) and (d) Temperature dependence of resistance for RbV_3Sb_5 under different magnetic fields at 0.38 GPa and 28.8 GPa, respectively. Increasing the magnetic field gradually suppresses the superconducting transition. Inset: Temperature dependence of the upper field $\mu_0 H_{c2}$. The superconducting transition temperature T_c is defined as the 10% drop of the normal-state resistance ($T_c^{10\%}$). The red line shows the fitting of Ginzburg-Landau theory, $\mu_0 H_{c2}(T) = \mu_0 H_{c2}(0)[1-(T/T_c)^2]/[1+(T/T_c)^2]$.

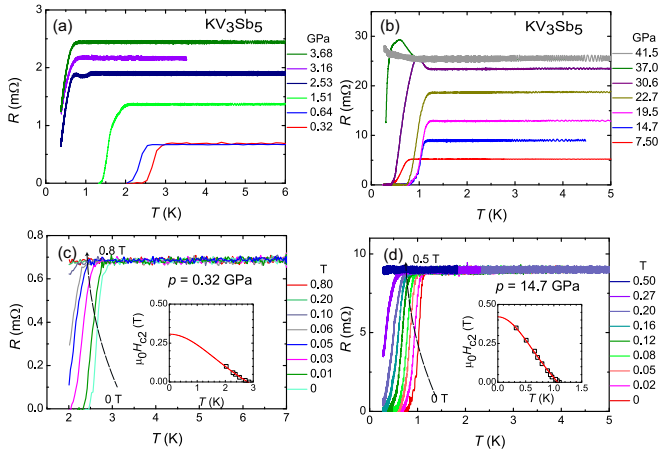

FIG. 3. (a) Temperature dependence of resistance for KV_3Sb_5 under various pressures up to 3.68 GPa. (b) Temperature dependence of resistance for KV_3Sb_5 under higher pressures up to 41.5 GPa. (c) and (d) Temperature dependence of resistance for KV_3Sb_5 under different magnetic fields at 0.32 GPa and 14.7 GPa, respectively. Inset: Temperature dependence of the upper field $\mu_0 H_{c2}$.

which is similar to that of CsV_3Sb_5 [14]. Below 3 GPa, a two-step-like transition is observed in the $R(T)$ curves, resembling the behavior at 0.61 and 0.90 GPa for CsV_3Sb_5, which was attributed to the presence of two superconducting phases [20]. It is likely a macroscopic phase separation due to pressure inhomogeneity inside the cell. By applying a slightly higher pressure, zero-resistance behavior reemerges and $T_c^{10\%}$ starts to increase with pressure to a maximum of 1.57 K at 28.8 GPa [Fig. 2(b)], showing a second superconducting dome.

To confirm that the resistance drop in RbV_3Sb_5 under pressures is superconducting transition, various magnetic fields are applied at 0.38 and 28.8 GPa [Figs. 2(c) and 2(d)]. The resistance drop is monotonically suppressed with increasing magnetic field as expected and completely vanishes in 1.5 T at 0.38 GPa and 1.4 T at 28.8 GPa, demonstrating that the resistance drop under pressure is indeed attributed to superconducting transition. The upper critical field ($\mu_0 H_{c2}$) versus $T_c^{10\%}$ of RbV_3Sb_5 at 0.38 and 28.8 GPa are summarized in the insets of Figs. 2(c) and 2(d). The data can be well fitted by the empirical Ginzburg-Landau (GL) formula $\mu_0 H_{c2}(T) = \mu_0 H_{c2}(0)[1-(T/T_c)^2]/[1+(T/T_c)^2]$. The $\mu_0 H_{c2}(0)$ are determined to be 0.86 and 1.06 T for 0.38 and 28.8 GPa, respectively. These values are much lower than the Pauli paramagnetic limit field $H_p(0) = 1.84 T_c \approx 7.6$ and 2.89 T, indicating the absence of Pauli pair breaking.

In analogy with that of RbV_3Sb_5, the resistance of KV_3Sb_5 under pressures is also measured and plotted in Fig. 3. Figures 3(a) and 3(b) show the low-temperature resistance of KV_3Sb_5 in the pressure range of 0.32–3.68 GPa and 7.5–41.5 GPa, respectively. Initially, the $T_c^{10\%}$ of KV_3Sb_5 increases sharply from 1.24 K at ambient pressure to 2.9 K at 0.32 GPa, which is, however, lower than those of RbV_3Sb_5 and CsV_3Sb_5 [14]. With increasing pressure, the resistance drop gradually moves towards lower temperature until reaches the minimum of 0.58 K at 3.68 GPa, which is similar to previous report [24]. Upon further compression, the $T_c^{10\%}$ increases to 1.14 K around 20 GPa followed with slow

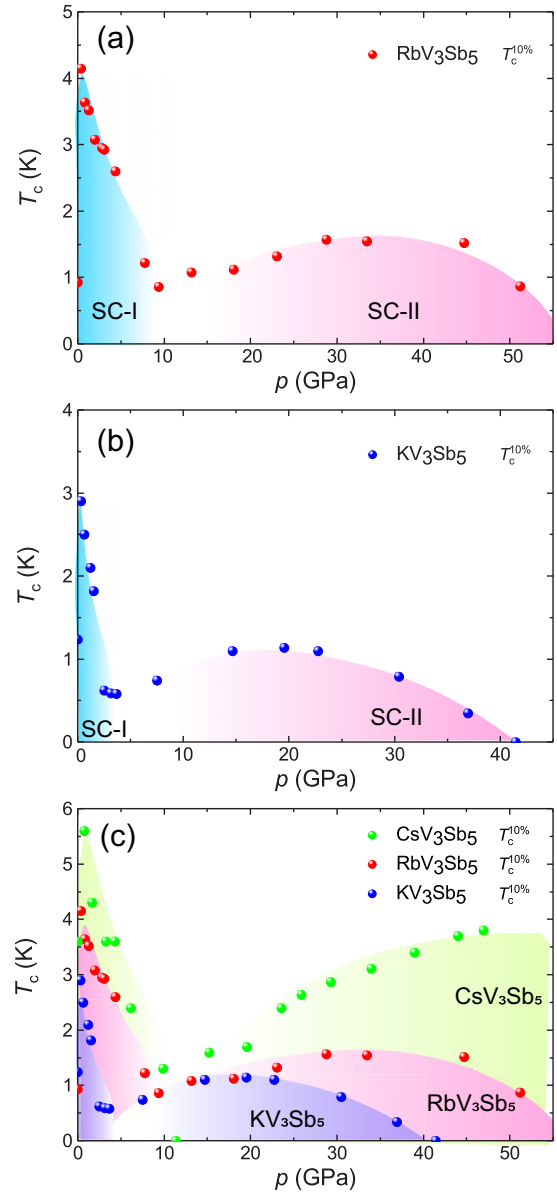

FIG. 4. Temperature-pressure phase diagram of (a) RbV_3Sb_5 and (b) KV_3Sb_5. Two superconducting domes can be clearly seen for both compounds, with SC-I phase under lower pressures and SC-II phase under higher pressures. (c) Temperature-pressure phase diagram of AV_3Sb_5 (A = Cs, Rb and K). The data of CsV_3Sb_5 are taken from our previous work [14]. The phase diagrams of CsV_3Sb_5, RbV_3Sb_5, and KV_3Sb_5 are colored with green, pink, and blue, respectively.

reduction and vanishes below 0.3 K at 41.5 GPa. Therefore, a second superconducting dome is also observed in KV_3Sb_5. Note that the transition is quite broad and an upturn manifests before the transition at 30.6 and 37.0 GPa, as seen in Fig. 3(b). Previously, such a peak has been observed in $L_{2-x}Ce_xCuO_4$ (L = Pr, Nd, Sm) single crystals, which was attributed to an intrinsic granularity of the crystal [25,26]. Here the broad transition and the peak should come from pressure inhomogeneity at high pressures, which causes the granularity.

The magnetic fields are applied to the sample at 0.32 and 14.7 GPa, as seen in Figs. 3(c) and 3(d). The resistance

drops completely suppresses at 0.8 T for 0.32 GPa and 0.5 T for 14.7 GPa. The $\mu_0 H_{c2}(T)$ can also be well fitted by GL equation, giving $\mu_0 H_{c2}(0) = 0.31$ and 0.42 T for 0.32 and 14.7 GPa [insets of Figs. 3(c) and 3(d)], respectively.

Based on above high-pressure resistance measurements of RbV_3Sb_5 and KV_3Sb_5, the temperature-pressure (T-p) phase diagrams are constructed in Figs. 4(a) and 4(b). Two superconducting domes can be clearly seen for both compounds, named as SC-I under lower pressures and SC-II under higher pressures. In SC-I phase, the T_c increases very rapidly at low pressure, as also being clearly observed in Ref. [24] in more detail. The rapid increase of T_c at low pressure is accompanied by a rapid decrease of T_{CDW}, which shows the competition between these two orders and reflects their underlying mechanisms [24]. In SC-II phase of KV_3Sb_5, the superconductivity persists up to 40 GPa, while in Ref. [24], it disappears already when pressure is higher than 30 GPa. This small inconsistency likely results from different transmitting medium, NaCl in this study vs. Daphne oil 7373 in Ref. [24], and/or slight difference in sample quality.

Therefore, all three compounds of AV_3Sb_5 (A = Cs, Rb, and K) have two superconducting domes under pressure, as a common feature. An integrated T_c–p phase diagram of V-based superconductors AV_3Sb_5 (A = Cs, Rb, and K) is summarized in Fig. 4(c). The high-pressure resistance data of CsV_3Sb_5 are taken from our previous work, Ref. [14]. One can see that CsV_3Sb_5 possesses the largest span phase diagram while KV_3Sb_5 possesses the smallest one among these V-based superconductors. With increasing the ionic radius of intercalated metal atoms from K to Cs, the maximum T_c in both SC-I and SC-II phases increases. The superconducting transition of CsV_3Sb_5 is also robust against pressure to more than 50 GPa in the second dome, whereas the superconducting transition of KV_3Sb_5 is undetectable at 41.5 GPa. Further experimental and theoretical works are needed to clarify the effect of different intercalated alkali-metal atoms on the superconductivity in AV_3Sb_5. Note that in the low-pressure regime, an unusual M-shaped T_c–p phase diagram of CsV_3Sb_5 with two peaks at 0.6 GPa and 2 GPa, was observed in the experiments with piston cylinder cell (PCC) and cubic anvil cell (CAC) [20,27]. In our previous measurements of CsV_3Sb_5 with DAC [14], we used relatively large pressure increment (only two data points below 2 GPa) to cover a wide pressure range. This is the reason why we do not resolve the unusual M-shaped phase diagram in the low-pressure regime.

Previously, the pressure-induced double-dome superconductivity was also observed in some other unconventional superconductors. The triggers of the second superconducting dome are categorized as: (i) first-order volume collapse or structural phase transition likely in the heavy-fermion superconductor $CeCu_2Si_2$ [28] and (ii) Lifshitz transition in the Fermi surface such as in iron chalcogenides [29,30] and cuprate superconductors [31]. In V-based superconductors CsV_3Sb_5 and KV_3Sb_5, the origin of the SC-I phase is strongly related to the CDW instability [14,20,24]. Since there is no any structural phase transition under pressure for CsV_3Sb_5, the SC-II phase was attributed to a pressure-induced Lifshitz transition and enhanced electron-phonon coupling in CsV_3Sb_5 [21,22]. The underlying superconducting pairing mechanism of these two superconducting domes needs further investigation.

In summary, we clarify the pressure dependence of superconductivity in the V-based superconductors AV_3Sb_5 (A = Rb and K). Two superconducting domes are unambiguously revealed in both compounds, as in CsV_3Sb_5, suggesting the pressure-induce double-dome superconductivity is a common feature in these V-based superconductors. The phase diagram is strongly affected by the ionic radius of intercalated alkali-metal atoms. These results shed a light on systemical understanding the superconducting pairing mechanism of V-based topological kagome metals.

This work was supported by the Natural Science Foundation of China (Grant No. 12174064), the Ministry of Science and Technology of China (Grant No. 2016YFA0300503), and the Shanghai Municipal Science and Technology Major Project (Grant No. 2019SHZDZX01). Y.F.G. was supported by the Major Research Plan of the National Natural Science Foundation of China (No. 92065201) and the Program for Professor of Special Appointment (Shanghai Eastern Scholar). H.C.L. was supported by the Ministry of Science and Technology of China (Grant No. 2018YFE0202600) and Beijing Natural Science Foundation (Grant No. Z200005).

[1] S. Yan, D. A. Huse, and S. R. White, Spin-liquid ground state of the $S = 1/2$ kagome Heisenberg antiferromagnet, Science **332**, 1173 (2011).

[2] W.-S. Wang, Z.-Z. Li, Y.-Y. Xiang, and Q.-H. Wang, Competing electronic orders on kagome lattices at van Hove filling, Phys. Rev. B **87**, 115135 (2013).

[3] M. L. Kiesel, C. Platt, and R. Thomale, Unconventional Fermi Surface Instabilities in the Kagome Hubbard Model, Phys. Rev. Lett. **110**, 126405 (2013).

[4] H.-M. Guo and M. Franz, Topological insulator on the kagome lattice, Phys. Rev. B **80**, 113102 (2009).

[5] I. I. Mazin, H. O. Jeschke, F. Lechermann, H. Lee, M. Fink, R. Thomale, and R. Valentí, Theoretical prediction of a strongly correlated Dirac metal, Nat. Commun. **5**, 4261 (2014).

[6] M. Kang, L. Ye, S. Fang, J.-S. You, A. Levitan, M. Han, J. I. Facio, C. Jozwiak, A. Bostwick, E. Rotenberg, M. K. Chan, R. D. McDonald, D. Graf, K. Kaznatcheev, E. Vescovo, D. C. Bell, E. Kaxiras, J. van den Brink, M. Richter, M. P. Ghimire, J. G. Checkelsky, and R. Comin, Dirac fermions and flat bands in the ideal kagome metal FeSn, Nat. Mater. **19**, 163 (2020).

[7] W.-H. Ko, P. A. Lee, and X.-G. Wen, Doped kagome system as exotic superconductor, Phys. Rev. B **79**, 214502 (2009).

[8] B. R. Ortiz, L. C. Gomes, J. R. Morey, M. Winiarski, M. Bordelon, J. S. Mangum, I. W. H. Oswald, J. A. Rodriguez-Rivera, J. R. Neilson, S. D. Wilson, E. Ertekin, T. M. McQueen, and E. S. Toberer, New kagome prototype materials: discovery of KV_3Sb_5, RbV_3Sb_5, and CsV_3Sb_5, Phys. Rev. Mater. **3**, 094407 (2019).

[9] B. R. Ortiz, S. M. L. Teicher, Y. Hu, J. L. Zuo, P. M. Sarte, E. C. Schueller, A. M. M. Abeykoon, M. J. Krogstad, S. Rosenkranz, R. Osbron, R. Seshadri, L. Balents, J. He, and S. D. Wilson, CsV_3Sb_5: A Z_2 Topological Kagome Metal with a Superconducting Ground State, Phys. Rev. Lett. **125**, 247002 (2020).

[10] B. R. Ortiz, P. M. Sarte, E. M. Kenney, M. J. Graf, S. M. L. Teicher, R. Seshadri, and S. D. Wilson, Superconductivity in the Z_2 kagome metal KV_3Sb_5, Phys. Rev. Mater. **5**, 034801 (2021).

[11] Q. W. Yin, Z. J. Tu, C. S. Gong, Y. Fu, S. H. Yan, and H. C. Lei, Superconductivity and normal-state properties of kagome metal RbV_3Sb_5 single crystals, Chin. Phys. Lett. **38**, 037403 (2021).

[12] Y.-X. Jiang, J.-X. Yin, M. M. Denner, N. Shumiya, B. R. Ortiz, G. Xu, Z. Guguchia, J. He, M. S. Hossain, X. Liu, J. Ruff, L. Kautzsch, S. S. Zhang, G. Chang, I. Belopolski, Q. Zhang, T. A. Cochran, D. Multer, M. Litskevich, Z.-J. Cheng *et al.*, Unconventional chiral charge order in kagome superconductor KV_3Sb_5, Nat. Mater. **20**, 1353 (2021).

[13] S.-Y. Yang, Y. Wang, B. R. Ortiz, D. Liu, J. Gayles, E. Derunova, R. Gonzalez-Hernandez, L. Šmejkal, Y. Chen, S. S. P. Parkin, S. D. Wilson, E. S. Toberer, T. McQueen, and M. N. Ali, Giant, unconventional anomalous Hall effect in the metallic frustrated magnet candidate, KV_3Sb_5, Sci. Adv. **6**, eabb6003 (2020).

[14] C. C. Zhao, L. S. Wang, W. Xia, Q. W. Yin, J. M. Ni, Y. Y. Huang, C. P. Tu, Z. C. Tao, Z. J. Tu, C. S. Gong, H. C. Lei, Y. F. Guo, X. F. Yang, and S. Y. Li, Nodal superconductivity and superconducting domes in the topological Kagome metal CsV_3Sb_5, arXiv:2102.08356.

[15] W. Duan, Z. Nie, S. Luo, F. Yu, B. R. Ortiz, L. Yin, H. Su, F. Du, A. Wang, Y. Chen, X. Lu, J. Ying, S. D. Wilson, X. Chen, Y. Song, and H. Yuan, Nodeless superconductivity in the kagome metal CsV_3Sb_5, Sci. China Phys. Mech. Astron. **64**, 107462 (2021).

[16] C. Mu, Q. W. Yin, Z. J. Tu, C. S. Gong, H. C. Lei, Z. Li, and J. L. Luo, *S*-wave superconductivity in kagome metal CsV_3Sb_5 revealed by $^{121/123}$Sb NQR and ^{51}V NMR measurements, Chin. Phys. Lett. **38**, 077402 (2021).

[17] H.-S. Xu, Y.-J. Yan, R. Yin, W. Xia, S. Fang, Z. Chen, Y. Li, W. Yang, Y. Guo, and D.-L. Feng, Multiband Superconductivity with Sign-Preserving Order Parameter in kagome Superconductor CsV_3Sb_5, Phys. Rev. Lett. **127**, 187004 (2021).

[18] B. R. Ortiz, S. M. L. Teicher, L. Kautzsch, P. M. Sarte, N. Ratcliffe, J. Harter, J. P. C. Ruff, R. Seshadri, and S. D. Wilson, Fermi Surface Mapping and the Nature of Charge Density Wave Order in the Kagome Superconductor CsV_3Sb_5, Phys. Rev. X **11**, 041030 (2021).

[19] X. Wu, T. Schwemmer, T. Müller, A. Consiglio, G. Sangiovanni, D. D. Sante, Y. Iqbal, W. Hanke, A. P. Schnyder, M. M. Denner, M. H. Fischer, T. Neupert, and R. Thomale, Nature of Unconventional Pairing in the Kagome Superconductors AV_3Sb_5 (A = K, Rb, Cs), Phys. Rev. Lett. **127**, 177001 (2021).

[20] K. Y. Chen, N. N. Wang, Q. W. Yin, Y. H. Gu, K. Jiang, Z. J. Tu, C. S. Gong, Y. Uwatoko, J. P. Sun, H. C. Lei, J. P. Hu, and J.-G. Cheng, Double Superconducting Dome and Triple Enhancement of T_c in the Kagome Superconductor CsV_3Sb_5 Under High Pressure, Phys. Rev. Lett. **126**, 247001 (2021).

[21] Z. Zhang, Z. Chen, Y. Zhou, Y. Yuan, S. Wang, J. Wang, H. Yang, C. An, L. Zhang, X. Zhu, Y. Zhou, X. Chen, J. Zhou, and Z. Yang, Pressure-induced reemergence of superconductivity in the topological kagome metal CsV_3Sb_5, Phys. Rev. B **103**, 224513 (2021).

[22] X. Chen, X. Zhan, X. Wang, J. Deng, X.-B. Liu, X. Chen, J.-G. Guo, and X. Chen, Highly robust reentrant superconductivity in CsV_3Sb_5 under pressure, Chin. Phys. Lett. **38**, 057402 (2021).

[23] Note that for Be-Cu DAC at low temperature around 4 K, the pressure is slightly higher than the value at room temperature. The pressure difference is negligible at 1 GPa, at most 1 GPa for 10 GPa, and at most 2 GPa for 20 GPa and 30 GPa. This is from private communication with Professor Liling Sun in the Institute of Physics, Chinese Academy of Science, who determined the pressure from Ruby at room temperature and from the superconducting transition temperature of Pb at low temperature.

[24] F. Du, S. S. Luo, B. R. Ortiz, Y. Chen, W. Y. Duan, D. T. Zhang, X. Lu, S. D. Wilson, Y. Song, and H. Q. Yuan, Pressure-induced double superconducting domes and charge instability in the kagome metal KV_3Sb_5, Phys. Rev. B **103**, L220504 (2021).

[25] M. A. Crusellas, J. Fontcuberta, and S. Pinol, Giant resistive peak close to the superconducting transition in $L_{2-x}Ce_xCuO_4$ single crystals, Phys. Rev. B **46**, 14089 (1992).

[26] S. Y. Li, W. Q. Mo, X. H. Chen, Y. M. Xiong, C. H. Wang, X. G. Luo, and Z. Sun, Low-temperature transport properties of $Nd_{2-x}Ce_xCuO_{4+\delta}$: Metal-insulator crossover in the overdoped regime, Phys. Rev. B **65**, 224515 (2002).

[27] F. H. Yu, D. H. Ma, W. Z. Zhuo, S. Q. Liu, X. K. Wen, B. Lei, J. J. Ying, and X. H. Chen, Unusual competition of superconductivity and charge-density-wave state in a compressed topological Kagome metal, Nat. Commun. **12**, 3645 (2021).

[28] H. Q. Yuan, F. M. Grosche, M. Deppe, C. Geibel, G. Sparn, and F. Steglich, Observation of two distinct superconducting phases in $CeCu_2Si_2$, Science **302**, 2104 (2003).

[29] L. Sun, X.-J. Chen, J. Guo, P. Gao, Q.-Z. Huang, H. Wang, M. Fang, X. Chen, G. Chen, Q. Wu, C. Zhang, D. Gu, X. Dong, L. Wang, K. Yang, A. Li, X. Dai, H.-K. Mao, and Z. Zhao, Re-emerging superconductivity at 48 kelvin in iron chalcogenides, Nature (London) **483**, 67 (2012).

[30] P. Shahi, J. P. Sun, S. H. Wang, Y. Y. Jiao, K. Y. Chen, S. S. Sun, H. C. Lei, Y. Uwatoko, B. S. Wang, and J.-G. Cheng, High-T_c superconductivity up to 55 K under high pressure in a heavily electron doped $Li_{0.36}(NH_3)_yFe_2Se_2$ single crystal, Phys. Rev. B **97**, 020508(R) (2018).

[31] L. Deng, Y. Zheng, Z. Wu, S. Huyan, H.-C. Wu, Y. Nie, K. Cho, and C.-W. Chu, Higher superconducting transition temperature by breaking the universal pressure relation, Proc. Natl. Acad. Sci. USA **116**, 2004 (2019).